THE ASTROPHYSICAL JOURNAL, 322:206–214, 1987 November 1

EVOLUTION OF 8–10 $M_\odot$ STARS TOWARD ELECTRON CAPTURE SUPERNOVAE. II. COLLAPSE OF AN O + Ne + Mg CORE[1]

KEN'ICHI NOMOTO
Department of Physics, Brookhaven National Laboratory; and
Department of Earth Science and Astronomy, University of Tokyo
Received 1987 January 13; accepted 1987 April 6

ABSTRACT

A helium core of an 8.8 $M_\odot$ star (initial core mass of 2.2 $M_\odot$) is evolved from the helium-burning stage through the early stage of collapse of an O + Ne + Mg core. The evolution is similar to the 9.6 $M_\odot$ star studied earlier; i.e., after nondegenerate carbon burning, the star forms a strongly degenerate O + Ne + Mg core because its mass, 1.28 $M_\odot$, is smaller than the critical mass for neon ignition. The penetration of the surface convection zone into the helium layer takes place earlier than in the 9.6 $M_\odot$ star, i.e., during carbon-burning phase. After most of the helium layer is dredged up, the degenerate core grows through the hydrogen-helium double-shell burning. When the mass interior to helium-burning shell (i.e., O + Ne + Mg core plus C + O layer) reaches 1.38 $M_\odot$, electron captures ^{24}Mg(e, ν)^{24}Na(e, ν)^{24}Ne, and ^{20}Ne(e, ν)^{20}F(e, ν)^{20}O start and induce the rapid contraction of the core. Entropy production associated with electron capture on ^{20}Ne as well as gravitational contraction leads to an ignition of the oxygen deflagration that incinerates the core material into nuclear statistical equilibrium (NSE). Electron capture in the NSE layer accelerates the collapse. Calculation is carried out through the neutrino trapping density. The star will become a Type II supernova to leave a neutron star less massive than 1.3 $M_\odot$. The effects of oxygen burning upon the hydrodynamic behavior of collapse and the possible nucleosynthetic yields are discussed.

Subject headings: nebulae: Crab Nebula — nucleosynthesis — stars: evolution — stars: interiors — stars: supernovae

I. INTRODUCTION AND SUMMARY

a) 8–10 $M_\odot$ Stars

As studied in an earlier paper (Nomoto 1984*a*; hereafter Paper I), the evolution of stars in the mass range of 8–10 $M_\odot$ is quite distinct from other mass ranges because 8–10 $M_\odot$ stars form strongly degenerate O + Ne + Mg cores after carbon burning. The simple modeling of the evolution of the O + Ne + Mg core has shown that the ultimate fate of these stars is the collapse of the core induced by electron captures on ^{24}Mg and ^{20}Ne (Miyaji *et al.* 1980, hereafter MNYS). In contrast, stars with masses smaller than 8 $M_\odot$ develop degenerate C-O cores and may either become white dwarfs by extensive mass loss or undergo thermonuclear explosion. Stars more massive than 10 $M_\odot$ burn carbon, neon, oxygen, and silicon under nondegenerate conditions; finally, the iron core collapses due primarily to photodisintegration of iron nuclei (see, e.g., Sugimoto and Nomoto [1980] for a review).

In Paper I, stars of 10.4 $M_\odot$ and 9.6 $M_\odot$ have been evolved from helium burning through the formation of an O + Ne + Mg core. The 10.4 $M_\odot$ star undergoes neon shell flash (see also Habets 1986). The 9.6 $M_\odot$ star, on the contrary, does not ignite neon because the mass of the O + Ne + Mg core is smaller than the critical mass of 1.37 $M_\odot$ for neon ignition. Afterward the O + Ne + Mg core of the 9.6 $M_\odot$ star becomes strongly degenerate. At the end of the calculation, the surface convection zone was found to penetrate into the helium layer.

In the present paper, a similar calculation is carried out for a slightly smaller mass, i.e., 8.8 $M_\odot$, star, from helium burning through the hydrodynamical stages of core collapse. (Preliminary results have been presented in Nomoto *et al.* 1982 and Nomoto 1984*b*.) Particular emphases are on the dredge-up phase and the final O + Ne + Mg core growth phase which have not been investigated before, and also on the transition stages from quasi-static through hydrodynamical stages induced by electron capture.

The calculation will confirm the earlier conclusion obtained from the simple core model that 8–10 $M_\odot$ stars eventually become electron capture supernovae (MNYS). It will be discussed how such presupernova evolution is common to the 8–10 $M_\odot$ range. The present calculation has provided an initial model for the supernova hydrodynamical calculation of the collapsing O + Ne + Mg core (Hillebrandt, Nomoto, and Wolff 1984; Burrows and Lattimer 1985; Baron, Cooperstein, and Kahana 1987; Mayle and Wilson 1987). Until recently, Type II supernova modeling has been tried mostly for iron cores in more massive stars (see, e.g., Hillebrandt 1982*a*; Wilson *et al.* 1985; Woosley and Weaver 1986 for reviews), although the importance to explore less massive stars is emphasized (Nomoto 1981; Hillebrandt 1982; Arnett 1982; Woosley and Weaver 1986). In view of the increasing interest in the 8–10 $M_\odot$ stars, it is necessary to present some details of the precollapse model of these stars.

b) Summary of Results

Through the present calculation, I have found that the 8.8 $M_\odot$ star evolves through the following stages. These results will be presented in detail section by section. (Input physics will be summarized in § II).

1. The star undergoes helium and carbon burning under nondegenerate conditions and leaves an O + Ne + Mg core. The mass of the O + Ne + Mg core is 1.28 $M_\odot$ so that no

[1] Supported in part by the US Department of Energy under Contract No. DE-AC02-76CH00016, and by the Japanese Ministry of Education, Science, and Culture through research grant No. 62540183.

neon ignition occurs. Such an evolution is very similar to that of the 9.6 $M_\odot$ star (§ III).

2. The penetration of the surface convection zone into the helium layer starts much earlier than in the 9.6 $M_\odot$ star, i.e., at the stage of central carbon burning. Most of the helium layer is dredged up (§ IV).

3. The subsequent evolution is brought about by the hydrogen-helium double-shell burning. The mass interior to the helium-burning shell (i.e., the mass of the O + Ne + Mg core plus the C + O layer), $M_{\rm Heb}$, increases toward the Chandrasekhar limit. The evolutionary track in the central density and temperature plane is determined mainly by the core growth rate and, hence, must be common to the 8–10 $M_\odot$ range (§ V).

4. After $M_{\rm Heb}$ reaches 1.375 $M_\odot$, electron captures on ^{24}Mg, ^{24}Na, ^{20}Ne, and ^{20}F take place. The electron concentration, Y_e, decreases, which induces the rapid contraction of the core (§ VI).

5. The rapid contraction of the core ignites the oxygen deflagration at the stage with the central density of $\rho_c > 10^{10}$ g cm^{-3}, and the material undergoes incineration into nuclear statistical equilibrium (NSE) at the oxygen deflagration front (§ VII).

6. The collapse of the core is accelerated owing to the rapid electron capture onto NSE elements. The oxygen deflagration front advances in mass to increase the mass of the NSE core (§ VII).

The calculation presented in this paper has stopped at $\rho_c = 3 \times 10^{11}$ g cm^{-3}. Subsequent stages of collapse, bounce, and shock propagation for this model have been calculated by Hillebrandt, Nomoto, and Wolff (1984); Burrows and Lattimer (1985); Baron, Cooperstein, and Kahana (1987); and Mayle and Wilson (1987). Hillebrandt, Nomoto, and Wolff (1984) found that the shock wave generated at the bounce does not damp as it propagates outward and successfully gives rise to a supernova explosion leaving a neutron star behind. On the contrary, the other three groups did not find such a prompt explosion. Mayle and Wilson (1987) found a delayed explosion due to late-time neutrino heating. These results suggest that the hydrodynamical outcome from 8–10 $M_\odot$ stars may be sensitive to various factors such as presupernova evolution, input physics, etc., as will be discussed in § VIII. Some features of nucleosynthesis will also be discussed in § IV which may be a clue to understanding the progenitor of the Crab Nebula (Nomoto 1982*c*, 1983; Nomoto *et al.* 1982).

II. METHOD OF CALCULATION AND INPUT PHYSICS

a) Models

As described in Paper I, the 8.8 $M_\odot$ star is divided into the hydrogen-rich envelope and the core at the hydrogen-burning shell (active or inactive). A Henyey-type calculation is carried out for the evolution of the core. The static hydrogen-rich envelope is calculated with the initial abundances of $X = 0.602$ and $Z = 0.02$ (Nomoto and Sugimoto 1972; Nomoto 1974) and fitted to the core at the hydrogen-burning shell. For convective layer in the envelope, the mixing length is assumed to be equal to a unit scale height of pressure. During the dredge-up of a helium layer, the abundances of the envelope is changed accordingly. For the double-shell burning phase, the approximated boundary conditions at the hydrogen-burning shell are applied as described in Paper I.

b) Input Physics

Henyey-type implicit hydrodynamical code and the input physics are mostly the same as used in Paper I and Nomoto (1982*a*, *b*) except for the following.

The equation of state for high-density core is updated to include the effects of strongly coupled plasmas (Slattery, Doolen, and DeWitt 1982). For the NSE layer of the collapsing core, the equation of state by Wolff (1984; see also Hillebrandt, Nomoto, and Wolff 1984) including 450 species is used.

For weak interactions in the degenerate O + Ne + Mg core, we used the same electron capture rates for ^{24}Mg, ^{24}Na, ^{20}Ne, ^{20}F, ^{16}O, etc., as given by MNYS. For the NSE layer, electron capture rates by Fuller, Fowler, and Newman (1982) are applied to the NSE composition (Yokoi, Neo, and Nomoto 1979; Nomoto, Thielemann, and Yokoi 1984; Thielemann, Nomoto, and Yokoi 1986).

III. EVOLUTION FROM HELIUM BURNING THROUGH FORMATION OF AN O + Ne + Mg CORE

The initial mass of the helium core of the 8.8 $M_\odot$ star was assumed to be 2.2 $M_\odot$, so that the present case is called as case 2.2 corresponding to case 2.4 ($M = 9.6$ $M_\odot$) and case 2.6 ($M = 10.4$ $M_\odot$) in Paper I. The calculation was started from the stage of central helium burning. The evolutionary stages are characterized by the change in masses contained interior to the shell of the maximum energy generation, E_n, for hydrogen ($M_{\rm Hb}$), helium ($M_{\rm Heb}$), and carbon ($M_{\rm Cb}$) burning as summarized in Table 1.

The chemical evolution of the core through the end of the dredge-up of helium layer is shown in Figure 1. The time, t, is measured from the end of the dredge-up and $t^* = -t$. The curled regions are convective due to nuclear burning, and the shaded region indicates a penetrating surface convection zone. Evolutionary changes in the photon luminosity at the outer edge of the core, $L_{\rm ph}$, the nuclear energy generation rate, L_n, and the neutrino luminosity, L_ν, are shown in Figure 2. Figure 3 shows changes in the physical quantities in the core, i.e., density (ρ_c), temperature (T_c), and chemical potential of an electron (ψ_c) in units of kT at the center. For the stages where

TABLE 1

EVOLUTIONARY STAGES AND CORE MASSES

CASE 2.2 (Stage)	TIME[a] (t^*[yr])	CORE MASSES ($M_\odot$)[b]		
		$M_{\rm Hb}$	$M_{\rm Heb}$	$M_{\rm Cb}$
Beginning of helium burning	2.22 E6	2.20	0.00	...
Helium exhaustion	2.83 E5	2.38	0.82	...
Carbon ignition	8.15 E4	2.38	1.11	0.21
Onset of the 1st dredge-up of the helium layer	4.89 E4	2.37	1.24	0.00
Carbon exhaustion	2.21 E4	1.50	1.27	0.57
1st peak of carbon shell burning	2.18 E4	1.49	1.27	0.60
2nd peak	7.80 E3	1.44	1.28	0.82
3rd peak	2.87 E3	1.44	1.28	0.91
4th peak	1.95 E3	1.44	1.28	1.10
Onset of the 2nd dredge-up of the helium layer	1.23 E3	1.43	1.28	1.11
5th peak of carbon shell burning	1.00 E3	1.42	1.28	1.14
6th peak	7.85 E2	1.41	1.28	1.19
Peak of helium shell burning	5.16 E2	1.40	1.28	1.21

[a] Time, $t^* = -t$, is measured from the end of dredge-up.

[b] Subscripts Hb, Heb, and Cb denote the shell of maximum energy generation of hydrogen, helium, and carbon burning, respectively.

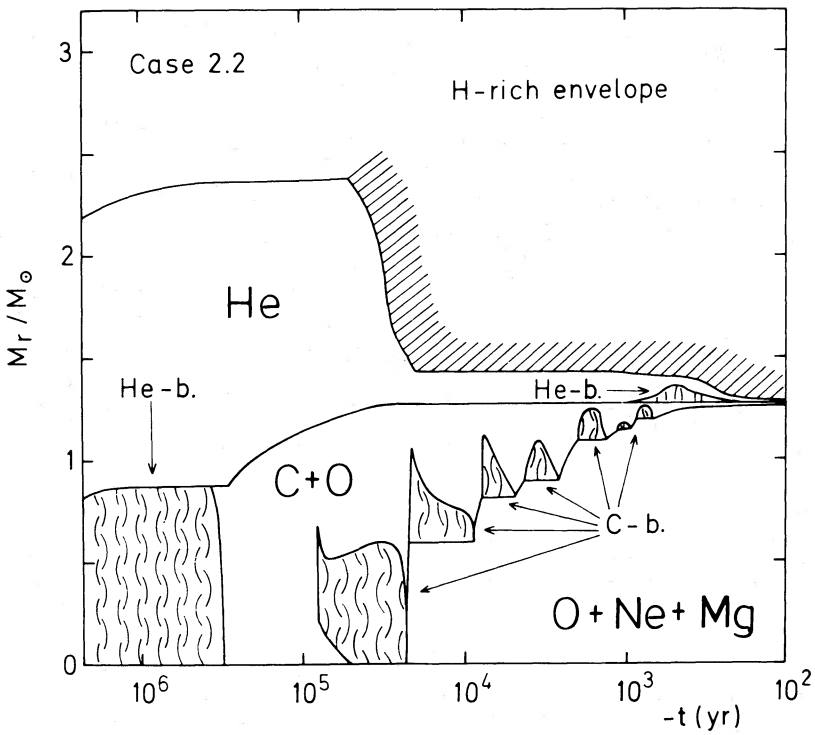

FIG. 1.—Chemical evolution of the helium core of initial mass 2.2 $M_\odot$ from core helium burning to the formation of O + Ne + Mg core. Time is measured backward from the end of the dredge-up of the helium layer. Convective regions due to helium and carbon burning are curled, and the surface convection zone is shaded.

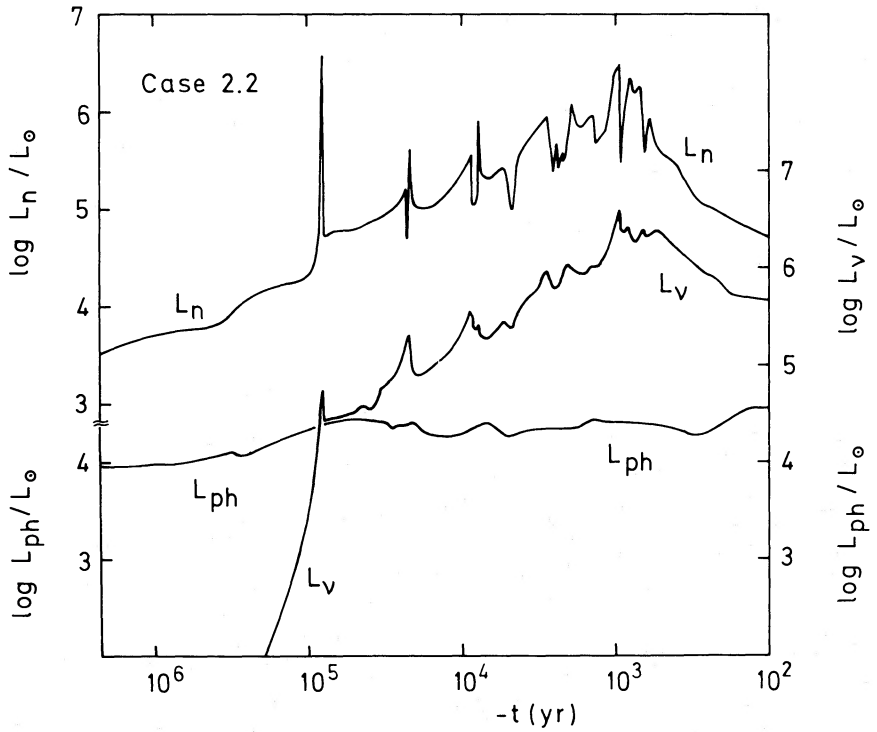

FIG. 2.—Evolutionary changes in the photon luminosity, L_{ph}, the nuclear energy generation ratio L_n, and the neutrino luminosity L_ν. Time is measured as in Fig. 1. Irregular behavior is due to weak carbon flashes.

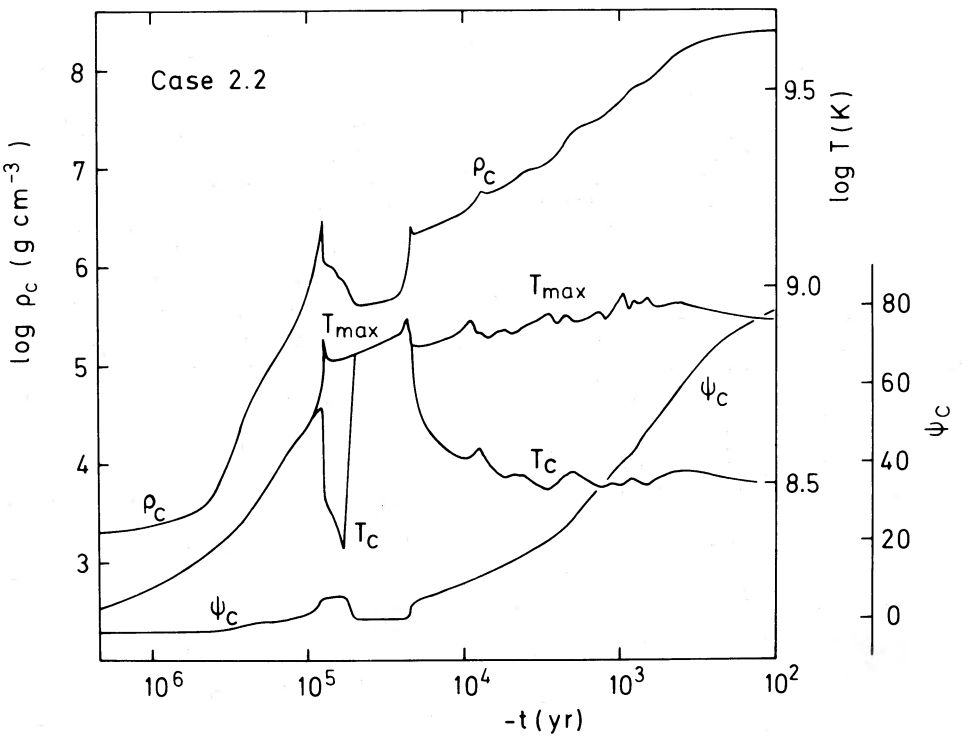

FIG. 3.—Evolutionary changes in the central density, ρ_c, temperature, T_c, and electron chemical potential, ψ_c, in units of kT. Time is measured as in Fig. 1. For stages where the temperature maximum appears in the outer shell, both the central temperature and the maximum temperature are shown.

the temperature inversion appears in the core, the maximum temperature within the core, T_{max}, is also plotted. The evolutionary track in the ρ_c and T_c plane is shown in Figure 4 through the stages of core collapse.

a) Helium and Carbon Burning

The qualitative features during helium burning, gravitational contraction of C + O core, and carbon burning are not much different from those found in Paper I, which are summarized as follows.

After core helium burning, the C + O core contracts and loses entropy mainly via neutrino emission. The core then becomes somewhat degenerate. The neutrino cooling rate is higher at higher density in the core, so that a temperature inversion is produced in the semidegenerate central region. This leads to off-center ignition of carbon at the shell of $M_r = 0.21\ M_\odot$. After a weak off-center flash, the carbon-burning layer moves inward because the inner layer is heated up to the carbon ignition temperature by energy transport from the burning layer.

During this phase, the evolutionary track in the (ρ_c, T_c)-plane makes a loop around $\rho_c = 10^6$ g cm^{-3} (Fig. 4).

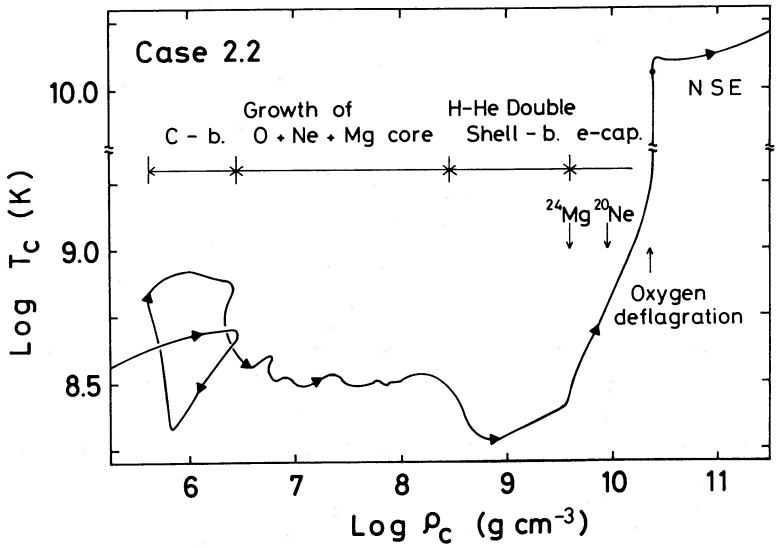

FIG. 4.—Evolutionary track in the central density and temperature diagram

Immediately after the shell flash, both ρ_c and T_c decrease because the flash leads to an almost adiabatic expansion of the core (Fig. 4). Afterward, T_c is increased as heat is transported from outer layers into the central region. Eventually carbon burning is ignited at the center when $\rho_c = 4 \times 10^5$ g cm^{-3} and $T_c = 7 \times 10^8$ K and proceeds under nondegenerate conditions.

There are some quantitative differences from the 9.6 $M_\odot$ star. Because of smaller core mass, central entropy is lower, i.e., ρ_c is higher and T_c is lower than in the 9.6 $M_\odot$ star at the same evolutionary stage. When a temperature inversion appears, the shell of maximum temperature locates at the shell of larger M_r. Accordingly, the carbon ignition occurs at the shell of larger M_r than in the 9.6 $M_\odot$ star.

b) *Growth of a Degenerate* O + Ne + Mg *Core*

After exhaustion of carbon in the central region, an O + Ne + Mg core is formed. Its mass, M_{Cb}, increases through carbon-shell burning (Fig. 1). (Irregular behavior of carbon-shell burning which forms a convective shell is discussed in detail in Paper I.) Figure 5 shows evolutionary changes in the radial distances from the center for several Lagrangian shells. Here the dotted regions are convective due to carbon burning. It is seen that the carbon-burning shell is almost stationary at $r = 0.01\ R_\odot$; the core materials contract being heated up to the carbon ignition and pass through the burning shell being processed from C + O to O + Ne + Mg. In this way, ρ_c increases as the mass of O + Ne + Mg core increases. At the same time, the central temperature decreases down to $\sim 3 \times 10^8$ K owing to neutrino emission. Accordingly, the core becomes strongly degenerate. At the end of the dredge-up phase, $M_{Cb} = 1.28\ M_\odot$, $\rho_c = 3 \times 10^8$ g cm^{-3}, $T_c = 3 \times 10^8$ K, and $\psi_c = 90$.

The maximum temperature ($\sim 8 \times 10^8$ K) first appears at the carbon-burning shell. When the carbon-burning shell gets close to the helium-burning shell at $t^* = 600$ yr, the shell of maximum temperature shifts to the O + Ne + Mg core. However, the peak value of temperature is 9×10^8 K, which is too low to ignite neon. This is because the mass of the O + Ne + Mg core is 1.28 $M_\odot$, that is, smaller than the critical values of 1.37 $M_\odot$ for neon ignition (Paper I).

We conclude that the evolution of the core is essentially the same as in the 9.6 $M_\odot$ star in the sense that the strongly degenerate O + Ne + Mg core is formed without neon ignition. The only quantitative difference is that M_{Cb} at the beginning of dredge-up is 1.28 $M_\odot$ for the 8.8 $M_\odot$ star, while it is 1.34 $M_\odot$ for the 9.6 $M_\odot$ star.

IV. CONVECTIVE DREDGE-UP OF HELIUM LAYER

a) *Expansion of a Helium Layer to Induce the Penetration of Surface Convection Zone*

As demonstrated in Paper I, the small O + Ne + Mg core mass, M_{Cb}, in 8–10 $M_\odot$ stars is essential to discriminating this mass range from more massive stars; i.e., M_{Cb} is smaller than 1.37 $M_\odot$ so neon is never ignited in the core. The small core mass leads to another important phenomenon at the interface between the core and envelope, i.e., penetration of the surface convection zone into the helium layer as found for the 9.6 $M_\odot$ star (Paper I).

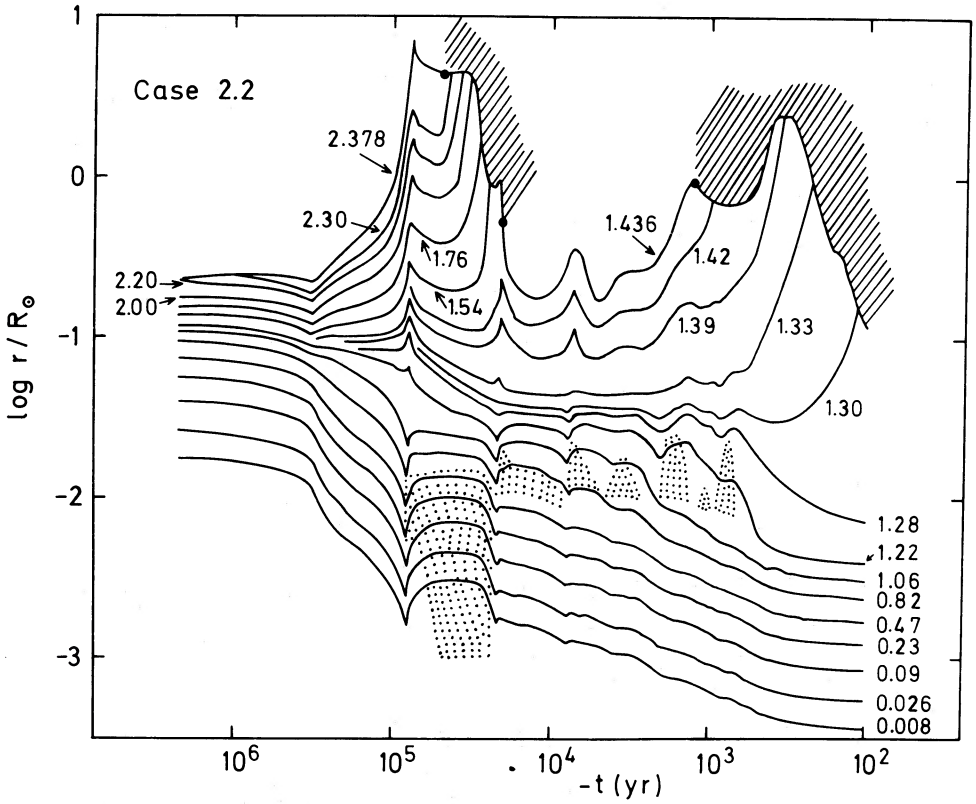

FIG. 5.—Evolutionary changes in the radial distances from the center for several Lagrangian shells indicated by $M_r/M_\odot$. Time is measured as in Fig. 1. Convective region due to carbon burning is indicated by dots, and the penetrating surface convection zone is shaded.

Such a penetration occurs when the material at the core edge absorbs much heat transported from the interior, and thus entropy thereof increases to exceed the entropy at the bottom of the surface convection zone (see Sugimoto and Nomoto [1974, 1980] for reviews). In other words, the penetration is induced by the expansion of a helium layer when the star develops a core-halo structure with an intervening burning shell as a node. Such an expansion is greater as the core is of a more centrally condensed type.

This is the reason why 5–8 $M_\odot$ stars undergo the dredge-up of helium layer when they develop strongly degenerate C + O cores: when the C + O core mass in these stars reaches about 1 $M_\odot$ and becomes highly condensed, the density at the helium-burning shell gets so low that the helium layer expands greatly. This induces a penetration of the surface convection zone (Paczyński 1970; Sugimoto 1971; Becker and Iben 1979; see Sugimoto and Nomoto 1980, p. 172 for details).

b) Progress of Dredge-up in 8–10 $M_\odot$ Stars

In the 9.6 $M_\odot$ star, the penetration starts when M_{Cb} reaches 1.24 $M_\odot$, and the O + Ne + Mg core becomes highly condensed. Paper I has shown that the helium layer expands greatly up to a red giant size if no dredge-up occurred.

In the 8.8 $M_\odot$ star the dredge-up starts significantly earlier, i.e., at the early stage of core carbon burning (Fig. 1). This is because the core is more condensed, while the outer part of the core is more extended in the 8.8 $M_\odot$ star than in the 9.6 $M_\odot$ star at carbon ignition. Contraction of the inner core and the expansion of the outer layers are seen in Figure 5.

The dredge-up of the helium layer proceeds as follows.

1. During the central carbon-burning phase, the dredge-up reduces the mass of the helium layer from 1.1 $M_\odot$ to 0.15 $M_\odot$, i.e., M_{Hb} decreases from 2.378 $M_\odot$ to 1.436 $M_\odot$. In the 9.6 $M_\odot$ star the dredge-up does not take place at this phase. (The dredge-up at similar phase in a 9 $M_\odot$ star was also reported by Weaver, Axelrod, and Woosley [1980], although they stopped calculating at early stage when only 0.3 $M_\odot$ of the helium layer had been dredged-up.)

2. During the several off-center carbon flashes, the surface convection zone temporarily retreats. Thus the dredge-up stops (see Fig. 1 and 5).

3. The dredge-up starts again when M_{Cb} grows to 1.11 $M_\odot$, i.e., the carbon-burning shell gets close to the helium-burning shell. This second dredge-up reduces the helium layer mass down to 5×10^{-3} $M_\odot$. The dredge-up that occurs in the 9.6 $M_\odot$ star (Paper I) corresponnds to this phase of dredge-up.

4. The surface convection zone retreats again when the hydrogen shell burning is ignited. At the termination of the dredge-up, M_{Hb} is 1.285 $M_\odot$.

The dredge-up rate is typically $dM_{Hb}/dt = -(1\text{–}2) \times 10^{-5}$ and $-(2\text{–}5) \times 10^{-5}$ $M_\odot$ yr^{-1} during the first and second dredge-up, respectively. The energy required for such a mixing of materials with different mean molecular weight per ion is 2×10^3–2×10^4 $L_\odot$ (see e.g., Becker and Iben 1980). This amounts to 10%–30% of the surface luminosity and is taken into account in the present calculation. The resulting decrease in the stellar luminosity leads to the enhancement of mixing because entropy at the bottom of the convective envelope is lower for lower luminosity (Nomoto and Sugimoto 1972; Nomoto 1974).

During the second dredge-up, a relatively small helium shell flash occurs. The size of the helium-burning convection zone is much smaller in mass than in the 9.6 $M_\odot$ and 10.4 $M_\odot$ stars (Fig. 1). In other words the dredge-up of the helium layer prevents the convective helium-shell burning from developing. As a result, mass of carbon mixed into the surface convection zone is as small as 0.007 $M_\odot$, which is one-third of the amount in the 9.6 $M_\odot$ star. Such a role by the dredge-up may be important in comparing the abundances of the helium layer with carbon abundance of the Crab Nebula (Nomoto 1982*c*, 1983; Nomoto *et al.* 1982).

V. DOUBLE SHELL BURNING AND THE GROWTH OF O + Ne + Mg CORE

a) Hydrogen-Helium Double-Shell Burning and Carbon-Shell Burning

After hydrogen-shell burning is ignited at the end of the dredge-up, helium layer is gradually built up. This is almost the same as occurs in degenerate C+O cores in 5–8 $M_\odot$ stars just after the second dredge-up phase (Sugimoto and Nomoto 1974, 1975; Iben 1975; Becker and Iben 1980). In 5–8 $M_\odot$ stars, the helium shell flash is eventually ignited when a sufficiently thick helium layer is built up. Afterward, the following events recur many times; thermal pulse of helium-shell burning, expansion of the helium layer, dredge-up by surface convection zone, ignition of hydrogen-shell burning, building up of a helium layer, and the next thermal pulse. This cycle reaches a limit cycle (Sugimoto and Miyaji 1981), and it increases the core mass.

The same type of the cycle may recur in the helium layer above the O + Ne + Mg core. In the present calculation the steady hydrogen-helium burning was assumed as has been done by Sugimoto and Nomoto (1975).

The subsequent evolutionary change in the chemical structure of the core is shown in Figure 6 as a function of the increasing central density. The hydrogen-helium double-shell burning advances in mass. The mass of helium layer is getting

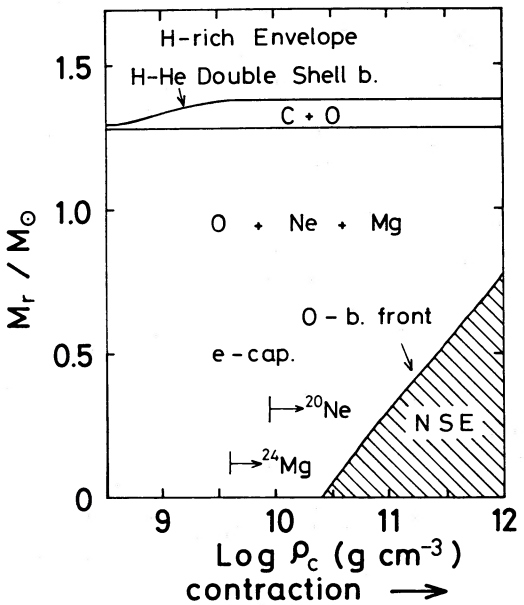

FIG. 6.—Chemical evolution after the end of the dredge-up is shown as a function of increasing central density. Growth of the C + O layer and electron capture leads to the contraction of the core, i.e., the increase in the central density. After the ignition of oxygen burning, nuclear statistical equilibrium (NSE) core grows as the core collapses.

thinner from $4 \times 10^{-5}\ M_\odot$ at $M_{\rm Hb} = 1.285\ M_\odot$ through $4 \times 10^{-6}\ M_\odot$ at $M_{\rm Hb} = 1.375\ M_\odot$; thus $M_{\rm Heb} \approx M_{\rm Hb}$.

As a result of the double-shell burning, a C + O layer gradually grows above the O + Ne + Mg core of 1.285 $M_\odot$. The temperature at the bottom of the C + O layer decreases to extinguish shell carbon burning because of neutrino emission. In order to increase the temperature thereof by compressional heating, the rate of core growth should be as high as $dM_{\rm Hb}/dt > 3 \times 10^{-6}\ M_\odot\ {\rm yr}^{-1}$ as found in the accreting white dwarf models (Nomoto and Iben 1985). The compressional heating in 8–10 $M_\odot$ stars is too small to keep carbon-shell burning active. In other words, formation of triple-shell burning (H, He, C) is not realized.

b) Common Evolutionary Track in the Central Density and Temperature

During the double-shell burning phase, the core mass to luminosity relation is close to Paczyński's relation (1970) for C + O cores. (If longer mixing length is assumed in the convective envelope, its bottom is deeper and the luminosity must be slightly higher; see Sugimoto and Nomoto 1974.) The growth rate of $M_{\rm Hb}$ is $dM_{\rm Hb}/dt = (7\text{–}8) \times 10^{-7}\ M_\odot\ {\rm yr}^{-1}$ in the present range of $M_{\rm Hb}$.

As $M_{\rm Hb}$ increases, the core contracts and ρ_c increases, as seen in Figure 6. Despite the composition difference in the interior to the double-burning shell, the relation between ρ_c and $M_{\rm Hb}$ is close to that for C + O cores. This implies that the compressional heating rate in the central region is almost the same as in C + O cores because of the similar $dM_{\rm Hb}/dt$.

The change in the central temperature during the double-shell burning phase is seen in Figure 4. This evolutionary track is determined by the competition between the neutrino loss and the compressional heating. Until $\rho_c \sim 10^9$ g cm^{-3} is reached, T_c decreases due to the neutrino loss. Afterward, the track approaches the common track for C + O cores (Paczyński 1970) being slightly below it because of the similar $dM_{\rm Hb}/dt$ and the slightly larger neutrino loss rate for O + Ne + Mg.

The temperature structure in the core is also determined by the compression and neutrino cooling. A temperature maximum appears at $M_r/M_{\rm Hb} = 0.9$ where the plasmon neutrino loss rate is low. In the central region, the neutrino bremsstrahlung is dominant and the temperature decreases outward.

The evolution of the core during the double-shell burning phase may be common to 8–10 $M_\odot$ stars because it is determined mainly by the growth rate of $M_{\rm Hb}$ and depends only weakly on the envelope mass (see Sugimoto and Nomoto 1980, p. 177). Therefore, the final fate of the star may also be common to this mass range except for the possibility of extensive mass loss to form O + Ne + Mg white dwarfs in lower mass range (Paper I).

VI. ELECTRON CAPTURES AND RAPID CONTRACTION OF THE O + Ne + Mg CORE

a) Onset of Electron Captures and Semiconvection

When $M_{\rm Hb}$ grows to as large as 1.376 $M_\odot$, the central density reaches 4×10^9 g cm^{-3}, for which the Fermi energy of degenerate electrons exceeds the threshold for the electron capture, $^{24}{\rm Mg}(e^-, \nu)^{24}{\rm Na}$. An electron is captured at first to form the isomeric state of ^{24}Na, which decays to its ground state by emitting gamma-ray with $E_\gamma = 0.2$ MeV.

Electron captures, especially onto the excited states of daughter nuclei, produce much entropy by emitting γ-rays and distorting the electron distribution function (see MNYS and Sugimoto and Nomoto [1980] for details). Resulting temperature rise is faster at higher density because the electron capture is faster. As a result a superadiabatic temperature gradient, $\nabla > \nabla_{\rm ad}$, appears in the central region. At the same time electron captures reduce the number of electrons per baryon, Y_e. This produces a gradient of mean molecular weight per electron, Y_e^{-1}, with material smaller Y_e inside. As a result, central region becomes semiconvective (Nomoto 1984*b*; Mochkovich 1984; also Isern *et al.* [1983] for C + O white dwarfs). The semiconvective layer is overstable with a growth time scale of heat transport over a convective element (Kato 1966). This time scale must be very short in the present case because heat production due to electron capture is faster for higher temperature and forms a very steep temperature gradient, almost a discontinuous jump in temperature, in the central region. Therefore, to what extent the material is mixed in the semiconvection zone depends on the time scale of evolution and also on the temperature structure.

During the early phase, electron captures are slow enough for the convection to develop, but later will get more rapid than the convective mixing of the material. It is not yet well established how to obtain an accurate solution for the semiconvective layer, in particular for the case with sharp temperature gradient and varying evolutionary time scale. Moreover, the change in Y_e due to both electron capture and mixing strongly couples with the energy absorption or production in the region with high Fermi energies. In the present study, therefore, Schwarzschild criterion was adopted for convective instability throughout the evolution in order to investigate one of the extreme cases. The other extreme case where Ledoux criterion is assumed has been studied by Miyaji and Nomoto (1987), and the final outcome has been found to be similar to the present case.

b) Contraction of the Core Induced by Electron Captures

Entropy production due to $^{24}{\rm Mg}(e^-, \nu)^{24}{\rm Na}$ forms a central convective zone at the stage with $\rho_c = 3.7 \times 10^9$ g cm^{-3}. Though this density is slightly lower than the threshold density for $T = 0$, the electron captures take place owing to a finite temperature.

Electron capture processes $^{24}{\rm Na}(e^-, \nu)^{24}{\rm Ne}$ and $^{20}{\rm Ne}(e^-, \nu)^{20}{\rm F}(e^-, \nu)^{20}{\rm O}$ begin when ρ_c exceeds 5×10^9 and 9×10^9 g cm^{-3}, respectively. ^{20}F captures an electron immediately after it is formed because the threshold density is as low as 3.2×10^9 g cm^{-3}. Such successive electron captures efficiently reduce Y_e. These electrons captures produce a lot of heat via the γ-ray emissions from the excited state of daughter nuclei (see Fig. 2 in MNYS). Thus the convective region gradually extends as found in MNYS. Almost steady abundances are seen at $\rho_c = 6\text{–}10 \times 10^9$ g cm^{-3}, where exhaustion due to electron captures and a supply of fresh material due to mixing are balanced (see MNYS).

As Y_e decreases, the value of the Chandrasekhar mass is reduced. The core contraction is accelerated, although its time scale is determined by electron capture, and thus still much longer than the dynamical one. For example, $\tau_\rho = dt/d \ln \rho_c = 10^4$ s at $\rho_c = 10^{10}$ g cm^{-3}, which is more than 10^6 times longer than the free-fall time scale. However, τ_ρ gets as short as 2 s at $\rho_c = 2 \times 10^{10}$ g cm^{-3}.

In short, the evolution during electron capture phase is not much different from that described in MNYS.

VII. OXYGEN COMBUSTION AND THE NEUTRONIZATION IN THE COLLAPSING CORE

a) Initiation of Oxygen Deflagration

As a result of increasing ρ_c and T_c during the rapid contraction, oxygen burning is becoming more important as a heating process than electron capture. At $\rho_c = 2.4 \times 10^{10}$ g cm^{-3}, T_c reaches a deflagration point ($\sim 2 \times 10^9$ K) where the time scale of temperature rise becomes shorter than the dynamical time scale (Fig. 4). Afterward the material at the deflagration front is incinerated into NSE composition.

The nuclear energy release is 0.4 MeV per nucleon, which is only 4% of the electron Fermi energy. Therefore, the resulting thermal overpressure is too small to initiate an oxygen detonation.

The core then oscillates a few times with a period of milliseconds. In the NSE region electron captures mainly on protons proceed rather rapidly to reduce the overpressure. The time scale of electron capture at this stage is ~ 0.1 s. Eventually the core begins to contract.

The core contraction leads to the increase in density and temperature ahead of the front up to the deflagration temperature. The oxygen deflagration front then advances in mass. In Eulerian coordinates, the deflagration front is almost stationary at a radius of ~ 170 km, and the infalling material goes through the front undergoing incineration into NSE. In this way the NSE core grows as ρ_c increases (shaded region in Fig. 6).

In the NSE core, electron capture accelerates the contraction. However, it is still slower than the free fall even at $\rho_c = 2 \times 10^{11}$ g cm^{-3}. Such a slow collapse is very different from iron cores in more massive stars.

b) Neutronization During Collapse

The ultimate fate of the collapsing core is either the formation of a neutron star by ejecting the outer layer or a continuing collapse into a black hole. This problem has been extensively studied for iron cores in stars more massive than 10 $M_\odot$ (see Hillebrandt [1982*a*] for a review). The analysis by Bethe *et al.* (1979) has shown that the crucial physical quantities to determine the final fate of the core collapse is Y_e and thus the rapidity of electron capture; this in turn depends on entropy, s_c, in the central region of the core, because electrons are captured primarily by free protons.

In the collapsing O + Ne + Mg core, the oxygen deflagration raises s_c up to as high as 1.3. Subsequent electron captures produce more entropy so that s_c reaches 1.4. Afterward s_c decreases to ~ 1.2 at the neutrino trapping density ($\sim 3 \times 10^{11}$ g cm^{-3}) because of the loss of high-energy neutrinos and nuclear dissociation. Electron captures reduce Y_e from 0.48 (at $\rho_c = 2.4 \times 10^{10}$ g cm^{-3}) to 0.35 ($\rho_c = 3 \times 10^{11}$ g cm^{-3}).

In the calculation where only the electron capture on protons is taken into account, s_c is slightly lower (~ 1.1) and Y_e higher (~ 0.36) at $\rho_c = 3 \times 10^{11}$ g cm^{-3} than above because of fewer electron captures.

Entropy is somewhat higher (and thus Y_e is lower) than the typical values found for iron core collapse in more massive stars (Hillebrandt 1982*a*). This will lead to a formation of a smaller homologous core during collapse and thus a formation of a weaker shock at bounce (Hillebrandt, Nomoto, and Wolff 1984; Burrows and Lattimer 1985; Baron, Cooperstein, and Kahana 1987; Mayle and Wilson 1987).

VIII. DISCUSSION AND CONCLUDING REMARKS

Main conclusions in the present study are summarized in § I. Among the recent improvements in the input physics is the increase of the $^{12}C(\alpha, \gamma)^{16}O$ reaction rate by a factor of ~ 3 (Fowler 1984). This reduces the ^{12}C abundance after helium burning and thus decreases the abundances of ^{20}Ne and ^{24}Mg. According to the new calculation with updated reaction rates (Caughlan *et al.* 1985) for 2.6 $M_\odot$ helium stars (Nomoto and Hashimoto 1987), $X(^{12}C) \approx 0.3$ and $X(^{16}O) \approx 0.7$ after helium burning and $X(^{16}O) \approx 0.54$, $X(^{20}Ne) \approx 0.37$, $X(^{23}Na) \approx 0.01$, $X(^{24}Mg) \approx 0.05$ after carbon burning. The abundances of our 2.2 $M_\odot$ helium core would be similar if new reaction rates were to be applied. Therefore, the degenerate core formed after carbon burning will be oxygen-rich rather than neon-rich as found in the present calculation. However, the amount of ^{24}Mg and ^{20}Ne required to reduce $\langle Y_e \rangle$ averaged over the central part of 0.6 $M_\odot$ is only $\Delta X \approx 0.15$. Therefore, the transition from quasi-static to hydrodynamic contraction should be almost the same as in the present study. Larger oxygen abundance leads to slightly larger nuclear energy release at the oxygen deflagration front. The effects on collapse will also be small.

As discussed in § VII, oxygen deflagration has some influence on the collapse. First, explosive nuclear energy release makes entropy of the NSE layer as high as 1.2, and it remains high because the cooling time scale by neutrino emission is longer than the collapse time scale. This leads to lower Y_e due to higher electron capture rates. As a result, homologous core mass, M_{HC}, at the bounce is smaller than in the iron core collapse case. For example, Hillebrandt, Nomoto, and Wolff (1984) found $M_{HC} \approx 0.64$ $M_\odot$, which is significantly smaller than 0.8 $M_\odot$ for the 20 $M_\odot$ star (Hillebrandt 1986). Since the energy transferred from the rebound core to the shock wave is smaller for smaller M_{HC} (e.g., Yahil 1983), the shock wave is weaker.

Second, explosive oxygen burning decelerates the infalling matter. The change in the infalling velocity amounts to $|\Delta v/v| \approx 0.3$ for the density at the burning front of 3×10^9 g cm^{-3} and ~ 0.1 for 1×10^{10} g cm^{-3}. This makes the density of the infalling matter lower. Therefore, the ram pressure ρv^2 is lower. This effect was found to be important by Hillebrandt, Nomoto, and Wolff (1984) but was insignificant in the calculations by other groups (Burrows and Lattimer 1985; Baron, Cooperstein, and Kahana 1987; Mayle and Wilson 1987). The difference in the density at the burning front may be due to the difference in the propagation velocity of the burning front, in these calculations.

Because of these competing effects of oxygen burning, the hydrodynamical behavior of collapse is sensitive to various factors involved in the hydrodynamical calculation, namely, the equation of state at high densities and the treatment of oxygen burning, etc. This may be the source of some discrepancies among the calculations.

Although there exists disagreement on the explosion energy, the ultimate fate of 8–10 $M_\odot$ stars will be Type II supernova explosion that leaves a neutron star remnant behind. The baryon mass of the neutron star M_A ranges from $M_A \sim 1.2$ $M_\odot$ for the prompt explosion model (Hillebrandt, Nomoto, and Wolff 1984) to $M_A \sim 1.33$ $M_\odot$ for the delayed model (Mayle

and Wilson 1987). The delayed explosion model also involve some uncertainties because the late time neutrino heating is sensitive to the neutrino temperature at the neutrinosphere (Bethe and Wilson 1985) and thus depends on the stiffness of the equation of state at high densities. In fact, Hillebrandt (1986) did not find a delayed explosion for the 20 $M_\odot$ star. In any case, the formation of a neutron star of $M_A > 1.38\ M_\odot$ is unlikely because of very steep density gradient at $M_r = 1.38\ M_\odot$ and a small binding energy ($\sim 10^{49}$ ergs) of extended hydrogen-rich envelope; even a weak explosion can eject such a weakly bound extended envelope. Therefore, the gravitational mass of neutron stars formed from 8–10 $M_\odot$ stars is smaller than 1.3 $M_\odot$.

Because of the uncertainty in the explosion mechanism, the nucleosynthesis products from 8–10 $M_\odot$ stars is not certain. If a significant amount of core material is processed by shock wave and ejected, it must be composed mostly of iron peak elements and even heavier elements (see Mayle and Wilson [1987] for the delayed model) because intermediate mass elements (Ca, Ar, S, Si, etc.) will be produced in the C + O layer with $\rho < 2 \times 10^6$ g cm^{-3} (Sugimoto and Nomoto 1980, p. 200) which includes only $\sim 10^{-4}\ M_\odot$. These iron peak elements would be somewhat neutron-rich because of electron captures after the passage of shock wave (Mayle and Wilson 1987). In this connection, large Ni to Fe ratio in the Crab Nebula reported by Dennefeld and Pequignot (1983) and by Henry (1984) are interesting. If such large Ni/Fe ratio is the abundance effect, not the effect of atomic physics, it would provide important information on the mass cut that divides the neutron star remnant and ejecta for the Crab Nebula's progenitor (Henry 1984).

The rest of the ejecta is mostly H-He envelope whose abundance depends on convective helium-shell burning and the mixing of the hydrogen-rich envelope and a helium layer. If the stellar mass has been reduced to $\sim 4\ M_\odot$ at the mixing phase, a relatively helium-rich layer is formed. Abundances of CNO elements and neon in this H-He layer are crucial in identifying the Crab Nebula's progenitor (Arnett 1975; Woosley *et al.* 1980; Nomoto 1985). The CNO abundances for 8–10 $M_\odot$ stars are not much enhanced and thus may be consistent with the Crab Nebula's progenitor (see Nomoto *et al.* [1982] for details).

Generally speaking, stars around 9 $M_\odot$ do not contribute much to the galactic nucleosyntheses. However, these stars might be sources of some rare species (Mayle and Wilson 1987). To clarify this detailed hydrodynamical and nucleosynthesis calculation is required.

I would like to thank R. G. Wolff, W. Hillebrandt, and K. Yokoi for providing me the equation of state and other input physics at high densities and for useful comments. It is a pleasure to thank S. H. Kahana, G. E. Brown, A. Yahil, A. Burrows, J. Cooperstein, and E. Baron for stimulating discussion and hospitality during my stay in Brookhaven and Stony Brook.

REFERENCES

Arnett, W. D. 1975, *Ap. J.*, **195**, 727.
———. 1982, *Ap. J. (Letters)*, **236**, L55.
Baron, E., Cooperstein, J., and Kahana, S. H. 1987, *Ap. J.*, **320**, 300.
Becker, S. A., and Iben, I., Jr. 1979, *Ap. J.*, **232**, 831.
———. 1980, *Ap. J.*, **237**, 111.
Bethe, H., Brown, G. E., Applegate, J., and Lattimer, J. M. 1979, *Nucl. Phys.*, **A324**, 487.
Bethe, H., and Wilson, J. R. 1985, *Ap. J.*, **295**, 14.
Burrows, H., and Lattimer, J. M. 1985, *Ap. J. (Letters)*, **299**, L19.
Caughlan, G. R., Fowler, W. A., Harris, M. J., and Zimmerman, B. A. 1985, *Atomic and Nuclear Data Tables*, **32**, 197.
Dennefeld, M., and Pequignot, D. 1983, *Astr. Ap.*, **127**, 42.
Fowler, W. A. 1984, *Rev. Mod. Phys.*, **56**, 149.
Fuller, G. M., Fowler, W. A., and Newman, M. 1982, *Ap. J. Suppl.*, **48**, 279.
Habets, G. M. H. J. 1986, *Astr. Ap.*, **167**, 61.
Henry, R. B. C. 1984, *Ap. J.*, **281**, 644.
Hillebrandt, W. 1982*a*, in *Supernovae: A Survey of Current Research*, ed. M. J. Rees and R. J. Stoneham (Dordrecht: Reidel), p. 123.
———. 1982*b*, *Astr. Ap.*, **110**, L3.
———. 1986, in *High Energy Phenomena around Collapsed Stars* (Dordrecht: Reidel), in press.
Hillebrandt, W., Nomoto, K., and Wolff, R. G. 1984, *Astr. Ap.*, **133**, 175.
Iben, I., Jr. 1975, *Ap. J.*, **196**, 525.
Isern, J., Labay, J., Hernanz, M., and Canal, R. 1983, *Ap. J.*, **273**, 320.
Kato, S. 1966, *Pub. Astr. Soc. Japan*, **18**, 374.
Mayle, R., and Wilson, J. R. 1987, *Ap. J.*, submitted.
Miyaji, S., and Nomoto, K. 1987, *Ap. J.*, **318**, 307.
Miyaji, S., Nomoto, K., Yokoi, K., and Sugimoto, D. 1980, *Pub. Astr. Soc. Japan*, **32**, 303 (MNYS).
Mochkovitch, R. 1984, in *Problems of Collapse and Numerical Relativity*, ed. D. Bancel and M. Signore (Dordrecht: Reidel), p. 125.
Nomoto, K. 1974, *Prog. Theor. Phys.*, **52**, 453.
———. 1981, in *IAU Symposium 93, Fundamental Problems in the Theory of Stellar Evolution*, ed. D. Sugimoto, D. Q. Lamb, and D. N. Schramm (Dordrecht: Reidel), p. 295.
———. 1982*a*, *Ap. J.*, **253**, 798.
———. 1982*b*, *Ap. J.*, **257**, 780.
———. 1982*c*, in *Supernovae: A Survey of Current Research*, ed. M. J. Rees and R. J. Stoneham (Dordrecht: Reidel), p. 205.
Nomoto, K. 1983, in *IAU Symposium 101, Supernova Remnants and Their X-Ray Emission*, ed. J. Danziger and P. Gorenstein (Dordrecht: Reidel), p. 139.
———. 1984*a*, *Ap. J.*, **277**, 791 (Paper I).
———. 1984*b*, in *Stellar Nucleosynthesis*, ed. C. Chiosi and A. Renzini (Dordrecht: Reidel), p. 238.
———. 1985, in *The Crab Nebula and Related Supernova Remnants*, ed. M. C. Kafatos and R. B. C. Henry (Cambridge: Cambridge University Press), p. 97.
Nomoto, K., and Hashimoto, M. 1987, *IAU Colloquium 93, Cataclysimic Variables*, ed. H. Drechsel, Y. Kondo, and J. Rahe (Dordrecht: Reidel). in *Ap. Space. Sci.*, **131**, 395.
Nomoto, K., and Iben, I., Jr. 1985, *Ap. J.*, **297**, 531.
Nomoto, K., Sparks, W. M., Fesen, R. A., Gull, T. R. Miyaji, S., and Sugimoto, D. 1982, *Nature*, **299**, 803.
Nomoto, K., and Sugimoto, D. 1972, *Prog. Theor. Phys.*, **48**, 46.
Nomoto, K., Thielemann, F.-K., and Yokoi, K. 1984, *Ap. J.*, **286**, 644.
Paczyński, B. 1970, *Acta Astr.*, **20**, 47.
Slattery, W. L., Doolen, G. D., and DeWitt, H. E. 1982, *Phys. Rev.*, **A26**, 2255.
Sugimoto, D. 1971, *Prog. Theor. Phys.*, **45**, 761.
Sugimoto, D., and Miyaji, S. 1981, in *IAU Symposium 93, Fundamental Problems in the Theory of Stellar Evolution*, ed. D. Sugimoto, D. Q. Lamb, and D. N. Schramm (Dordrecht: Reidel), p. 191.
Sugimoto, D., and Nomoto, K. 1974, in *IAU Symposium 66, Late Stages of Stellar Evolution*, ed. R. J. Taylor (Dordrecht: Reidel), p. 105.
———. 1975, *Pub. Astr. Soc. Japan*, **27**, 197.
———. 1980, *Space Sci. Rev.*, **25**, 155.
Thielemann, F-K., Nomoto, K., and Yokoi, K. 1986, *Astr. Ap.*, **158**, 17.
Weaver, T. A., Axelrod, T. S., and Woosley, S. E. 1980, in *Type I Supernovae*, ed. J. C. Wheeler (Austin: University of Texas Press), p. 113.
Wilson, J. R., Mayle, R., Woosley, S. E., and Weaver, T. A. 1986, *Ann. Nat. Acad. Sci.*, **470**, 267.
Wolff, R. G. 1984, private communication.
Woosley, S. E., and Weaver, T. A. 1986, *Ann. Rev. Astr. Ap.*, **24**, 205.
Woosley, S. E., Weaver, T. A., and Taam, R. E. 1980, in *Type I Supernovae*, ed. J. C. Wheeler (Austin: University of Texas Press), p. 96.
Yahil, A. 1983, *Ap. J.*, **265**, 1047.
Yokoi, K., Neo, S., and Nomoto, K. 1979, *Astr. Ap.*, **77**, 210.

KEN'ICHI NOMOTO: Department of Earth Science and Astronomy, College of Arts and Sciences, University of Tokyo, Meguro-ku, Tokyo 153, Japan